LAWRENCE
LIVERMORE
NATIONAL
LABORATORY

UCRL-TR-214046

Final Report on California Regional Wind Energy Forecasting Project:Application of NARAC Wind Prediction System

Hung-Neng S Chin

July 27, 2005

This work was performed under the auspices of the U.S. Department of Energy by University of California, Lawrence Livermore National Laboratory under Contract W-7405-Eng-48.

Final Report on California Regional Wind Energy Forecasting Project: Application of NARAC Wind Prediction System

Hung-Neng S. Chin

National Atmospheric Release Advisory Center (NARAC)
Lawrence Livermore National Laboratory (LLNL)

1. Introduction

Wind power is the fastest growing renewable energy technology and electric power source (AWEA, 2004a). This renewable energy has demonstrated its readiness to become a more significant contributor to the electricity supply in the western U.S. and help ease the power shortage (AWEA, 2000). The practical exercise of this alternative energy supply also showed its function in stabilizing electricity prices and reducing the emissions of pollution and greenhouse gases from other natural gas-fired power plants.

According to the U.S. Department of Energy (DOE), the world's winds could theoretically supply the equivalent of 5800 quadrillion BTUs of energy each year, which is 15 times current world energy demand (AWEA, 2004b). Archer and Jacobson (2005) also reported an estimation of the global wind energy potential with the magnitude near half of DOE's quote.

Wind energy has been widely used in Europe; it currently supplies 20% and 6% of Denmark's and Germany's electric power, respectively, while less than 1% of U.S. electricity is generated from wind (AWEA, 2004a). The production of wind energy in California (~1.2% of total power) is slightly higher than the national average (CEC & EPRI, 2003). With the recently enacted Renewable Portfolio Standards calling for 20% of renewables in California's power generation mix by 2010, the growth of wind energy would become an important resource on the electricity network.

Based on recent wind energy research (Roulston et al., 2003), accurate weather forecasting has been recognized as an important factor to further improve the wind energy forecast for effective power management. To this end, UC-Davis (UCD) and LLNL proposed a joint effort through the use of UCD's wind tunnel facility and LLNL's real-time weather forecasting capability to develop an improved regional wind energy forecasting system.

The current effort of UC-Davis is aimed at developing a database of wind turbine power curves as a function of wind speed and direction, using its wind tunnel facility at the windmill farm at the Altamont Pass. The main objective of LLNL's involvement is to provide UC-Davis with improved wind forecasts to drive the parameterization scheme of turbine power curves developed from the wind tunnel facility. Another objective of LLNL's effort is to support the windmill farm operation with real-time wind forecasts for the effective energy management. The forecast skill in capturing the situation to meet the cut-in and cut-out speed of given turbines would help reduce the operation cost in low and strong wind scenarios, respectively.

The main focus of this report is to evaluate the wind forecast errors of LLNL's three-dimensional real-time weather forecast model at the location with the complex terrain. The assessment of weather forecast accuracy would help quantify the source of wind energy forecast errors from the atmospheric forecast model and/or wind-tunnel module for further improvement in the wind energy forecasting system.

2. Model and Experiment Design

A modified version of the Naval Research Laboratory's (NRL's) three-dimensional coupled Ocean / Atmosphere mesoscale prediction system (COAMPS) of version 2.0.15 is used in this study (Chin et al. 2000, 2001 and 2005). COAMPS consists of a data assimilation system, a nonhydrostatic atmospheric forecast model, and a hydrostatic ocean model.

In this study, we use only the data assimilation and the atmospheric model to provide real-time forecasts. The atmospheric forecast model is

* *Corresponding author address*: Dr. Chin, Lawrence Livermore National Lab. (L-103), Livermore, CA 94550; e-mail: chin2@llnl.gov.

composed of a compressible form of the dynamics, nest-grid capability, and parameterizations of subgrid-scale turbulence, surface momentum and heat fluxes, explicit ice microphysics, subgrid-scale cumulus clouds, shortwave and longwave radiation, and urban canopy physics. The terrain-following vertical coordinate is also used to simulate airflow over an irregular surface. The model terrain is given from 1-km resolution terrain database using Silhouette average method with filter. The reader is referred to Hodur (1997) for further details of COAMPS, and Chin et al. (2005) for newly implemented physics.

The model domain contains 31 grid points in the vertical, with the grid size varied to maximize resolution at lower levels. Totally, it contains 9 grid points below the altitude of 127 m with the corresponding grid spacing of 4, 4, 4, 6, 10, 16, 24, 34 and 50 m, respectively. The grid spacing aloft is gradually increased to 800 m at the altitude of 3.152 km. Above this level, a uniform grid size of 800 m is specified up to the altitude of 7.592km. Then, the grid size is further smoothly increased to 5.0 km with the domain top residing at 24.352km.

In the horizontal, a total of three nested domains are adopted in this study. Both zonal and meridional coordinates have 61 grid points for all nested grids. A uniform grid size of 36 km is used for the outer coarser mesh (nest_1) with a constant size ratio of three to define the inner nest grids. Therefore, the finest grid resolution of the third nested domain shown in this study is 4 km (nest_3).

Constant time steps of 90 and 45 seconds for non-sound and sound wave calculations, respectively, are used in the coarser grids for the time-splitting scheme. The time steps for the finer-grid domains are reduced proportionally to the nest-grid size ratios. The rigid boundary condition is imposed at the vertical boundary. A sponge-damping layer is placed above 10.052 km to minimize the reflection of internal gravity waves off the rigid upper boundary. The Davies (1976) boundary condition is applied to the lateral boundaries with a nudging zone of seven grid points at each lateral boundary. A time filter with a coefficient of 0.2 is applied to control computational instability associated with the leapfrog time approximation in the model.

In this study, two watches of 48-h forecasts (00Z and 12 Z, respectively) are performed daily over California with the center at the Altamont Pass for a total of 12 months from July 2004 to June 2005. However, due to the size limit of huge forecast data storage, only the data of all nested grids in the first week of each month are stored and used to assess the forecast errors with respect to the measurements at 11 available tower observations. Nonetheless, the yearly forecast data of the finest grids are stored at UC-Davis for a separate study to evaluate the wind energy forecast errors. The mean absolute errors of wind speed and direction at each forecast hour are shown in this study to avoid the canceling effect of under- and over-prediction via the averaging process.

3. Measurements for Model Validation

A total of 11 meteorological tower stations at the Altamont Pass are used to calculate the mean absolute forecast errors for wind speed and direction. These observations are available in 30-minute averages. The locations and the heights of tower measurements can be seen in Figure 1 and Table 1. All tower measurements are located at 18 meters above the ground, except for three stations; station 225 and 438 at 24 meters, and station 832 at 30 meters. The model forecast is interpolated to the same location as the observations in both horizontal and vertical (height above the ground) directions to compute the absolute forecast errors.

Quality assurance of tower measurements shows great uncertainty in the wind direction observations. In particular, the measured wind direction at station 624 reported a constant value of 0.3 ~ 0.5 throughout the year of interest. In the mean time, another 5 stations, such as 427, 821, 826, 832, and 922, exhibit a small range of fluctuation (few degrees) with respect to a wind angle around a few tens of degrees. This category of wind direction measurements may arise from the channeling effect of the local terrain, and does not necessarily imply poor quality. All of these 6 stations are referred to as uncertain (UNC) stations, and the remaining 5 stations with reliable wind direction measurements are referred

to as REL stations in this study. The separation of reliable and uncertain stations is also used to gauge its impact on the forecast errors.

4. Results

The mean absolute errors of forecast wind speed and direction shown in this study are derived for each month using the data at every forecast hour throughout the whole forecast period (i.e., 48 hours), and averaging over available tower stations and 14 forecasts (two watches per day for one week). Normally, these mean absolute errors are computed using the forecasts in the first week of each month. Occasionally, this duration period is shifted for several days to accommodate the availability of station measurements.

The forecast errors from a warm month (June 2005) clearly exhibit the dependence of wind speed error on the grid resolution using the data from all stations (Fig. 2a) while this impact is not seen in the wind direction error (Fig. 2b). The observed station wind speed of the warm month can be as strong as 20 m/s. The absolute error of forecast wind speed is about 6 m/s with the coarser grid resolution (36 km) while this error can be reduced to 4 m/s in the higher resolution forecast (4 km). With the separation of UNC and REL stations, the impact of grid resolution on wind speed errors remains unchanged (Figs. 2c and 2e). In contrast, the wind direction error is significantly reduced with increasing grid resolution using REL stations while this error is fairly large at UNC stations and shows an opposite dependence on the grid resolution (Figs. 2d and 2f).

In contrast, Figure 3 shows the forecast errors from a cold month (December 2004). The gross feature of resolution impact on the wind speed and direction in the cold month is very different from its warm-month counterpart; there is no clear dependence of forecast errors on grid resolution in the cold month, even with the separation of REL and UNC stations. In addition, the magnitude of wind speed errors is noticeably reduced in the cold month as a result of weaker wind (< 10 m/s, except for the storm period). Although the resolution impact is weak in the cold month, the separation of UNC and REL stations still exhibits qualitative improvement in the forecast error for both wind speed and direction. Therefore, only the results from the REL stations are shown for the rest of months under investigation to gauge a complete seasonal variation of forecast errors.

The detailed month-to-month variation of forecast errors is illustrated in Figs. 4, 5, 6, and 7 using the measurements from only REL stations. A noticeable change of grid resolution impact on the wind speed error appears at two transition times; (1) from October to November, and (2) from March to April. However, this resolution impact is not well detected in the forecast errors of wind direction for the warm months before October 2004. This result arises from the change of COAMPS physics in September 2004 due to the consideration of soil moisture impact on the re-distribution of surface latent and sensible heat fluxes, and its resulting development of planetary boundary layer. As a result, this new physics acts to improve the surface energy budget and its related surface temperature and wind forecast. Therefore, a clear grid resolution impact on the wind direction starts to appear in the warm months after October 2004. This new physics also has an effect in reducing the forecast errors of wind speed in the warm months.

As seen in Table 1, the finest resolution (4 km in the nest_3 domain) used in the simulations is still not enough; the resolved model terrain heights in the nest_3 domain at most of the measurement stations substantially differ from the reality. Our terrain database indicates that the model needs at least one more nest to properly represent the local terrain forcing for reducing the forecast errors.

To assess the impact of inaccurately modeled terrain forcing, the vertical profiles of forecast horizontal winds in a warm / cold month are illustrated in Fig. 8. The evolution of these forecast winds exhibits strong nocturnal winds at the Altamont Pass. The vertical wind shear in the lowest 100 meters is also large, particularly in the warm month. To estimate the quantitative impact of modeled terrain on forecast winds, the forecast errors for June 2005 and December 2004 with the terrain calibration (i.e., comparing forecast wind with measured at the actual station height) are shown in Fig. 9. As expected, the main

differences appear in the warm month, particularly in the wind speed error of an additional 1 m/s for each grid resolution. This suggests that simply improving the modeled terrain geometry is not sufficient to reduce the forecast errors.

The yearly forecast results clearly indicate that the forecast errors over the Altamont Pass area can be characterized by a semi-annual variation. In the warm months when the synoptic-scale front activity is weak, the model exhibits a strong grid resolution impact on the forecast accuracy as a result of the improved representation of local terrain with increasing grid resolution. In contrast, the cold months coincide with the prevailing frontal activity so that the local terrain becomes a secondary forcing for the model forecast. Therefore, there is no clear dependence of forecast errors on grid resolution. In addition, the large forecast error of wind direction in the cold months may arise from the improper model terrain geometry.

5. Summary

NARAC's real-time wind prediction system, COAMPS, is being used in conjunction with the wind tunnel facility at UC-Davis to develop an improved regional wind energy forecasting system. This weather forecast model provides a 48-h real-time prediction with horizontal resolutions from 36 km to 4 km over California with the center near the Altamont Pass with complex terrain. The forecast is performed twice a day (00Z and 12Z, respectively) for one year starting from July 1 2004. The model outputs are used to support both research and operation management. However, only the validation of COAMPS forecast is presented in this report. The evaluation of the overall wind energy forecasting system is covered by UC-Davis in a separate report.

The month-to-month variation of wind forecast errors clearly exhibits a semi-annual fluctuation with prominent dependence on the grid resolution in the warm months (i.e., strong wind power period) when the frontal activity is weak; the large forecast errors are systematically reduced with increasing grid resolution for both wind speed and direction. However, this dependence diminishes when synoptic-scale frontal activity prevails in the cold months.

The remaining question to be addressed from this research outcome is whether the grid resolution dependence would continue with decreasing grid size or if this dependence tendency converges at a certain grid size in the strong wind power period. Although the increasing grid resolution can resolve a better representation of model terrain geometry (magnitude and shape), further study of Silhouette terrain representation and the use of finer resolution terrain database are highly recommended to improve the forecast accuracy for the airflow over the complex terrain.

Due to the computational limitation of a shared memory model, it becomes infeasible to meet the real-time forecast requirement for simulations with further increased resolutions. The implication of this research strongly supports the value of high-performance computing to further improve the wind energy forecast. To this end, NARAC is in the transition to convert COAMPS to the distributed memory code to allow faster and higher resolution real-time forecast. Our recent test of MPI (message passing interface) COAMPS has shown its readiness for the operational use in the coming fall.

Acknowledgments. The author wishes to thank Electric Power Research Institute for providing tower measurements to validate the accuracy of model forecast. This work was supported by California Energy Commission wind energy forecasting project (Contract No. E2IP219C7619) and the U.S. Department of Energy (DOE) National Advisory Release Assessment Program at LLNL, and conducted under the auspices of the DOE by the University of California, Lawrence Livermore National Laboratory under Contract W-7405-Eng-48.

6. References

American Wind Energy Association (AWEA), Wind Energy Stands Ready to help Ease California Shortages, 2000. http://www.awea.org/news/news00101222ces.html, 2000.

American Wind Energy Association (AWEA), Global Market Report 2004a. http://www.awea.org/pubs/documents/globalmerket2004.pdf, 2004.

American Wind Energy Association (AWEA), Wind Energy potential 2004b. http://www.awea.org/faq/tutorial/wwt_potential.html, 2004.

Archer C. L., and M. Z. Jacobson, 2005: Evaluation of global wind power. *J. Geophys. Res*., (in press).

California Energy Commission (CEC) and Electrical Power Research Institution (EPRI), California Wind Energy Forecasting System Development and Testing Phase 2: 12-Month Testing, 1007339, 2003.

Chin, H.-N. S., M. J. Leach, and M. J. Brown, 2000: A preliminary study of the urban canopy effects on a regional-scale model: Sensitivity assessment of an idealized case. Proceedings of the third Symposium on the Urban Environment, July 14-18, 2000, Davis, California, *Amer. Meteor. Soc*., 76-77.

Chin, H.-N. S., M. J. Leach, G. Sugiyama, and F. J. Aluzzi, 2001: A Preliminary Study of Surface Temperature Cold Bias in COAMPS. Proceedings of the Ninth Conference on Mesoscale Processes, 30 July -2 August 2001, Fort Lauderdale, Florida, *Amer. Meteor. Soc*., 249-254.

Chin, H.-N. S., M. J. Leach, G. A. Sugiyama, J. M. Leone Jr., H. Walker, J. S. Nasstrom, and M. J. Brown, 2005: Evaluation of an urban canopy parameterization in a mesoscale model using VTMX and URBAN 2000 data. *Mon. Wea. Rev*., **133**, 2043-2068.

Hodur, R., 1997: The Naval Research Laboratory's coupled ocean-atmospheric mesoscale prediction system (COAMPS). *Mon. Wea. Rev.*, **125**, 1414-1430.

Roulston, M. S., D.T. Kaplan, J. Hardenberg, and L. A. Smith, 2003: Using Medium Range Weather Forecasts to improve the value of wind energy production. *Renewable Energy*, **28**, 585-602.

Table 1. Station information of tower measurements at the Altamont Pass. Station and modeled terrain heights are also shown for different grid resolutions.

Station	Sta_ID	Sta_lon(°)	Sta_lat(°)	Sta_H(m)	36km_H	12km_H	4km_H	1.33km_H	0.44km_H
1	127	-121.6927	37.764416	335.28	102.23	175.04	175.81	295.98	335.33
2	225	-121.6673	37.767766	312.42	101.32	179.34	159.22	254.75	256.50
3	427	-121.6285	37.717583	342.90	108.99	239.48	238.27	276.08	302.95
4	438	-121.6734	37.711416	415.75	110.25	225.73	223.38	272.39	304.52
5	624	-121.6836	37.729388	347.90	107.70	203.52	190.67	260.13	269.08
6	723	-121.6357	37.788916	198.12	98.47	166.03	119.07	122.31	147.58
7	821	-121.5997	37.701777	237.74	112.20	264.60	278.24	289.95	278.00
8	826	-121.5798	37.675527	419.10	116.72	300.48	349.88	394.08	460.91
9	832	-121.6141	37.680555	441.96	114.75	288.87	340.08	434.68	536.57
10	922	-121.6073	37.759777	121.92	103.84	193.14	145.17	117.46	125.04
11	926	-121.6316	37.738555	242.32	105.69	213.53	191.03	221.19	217.46

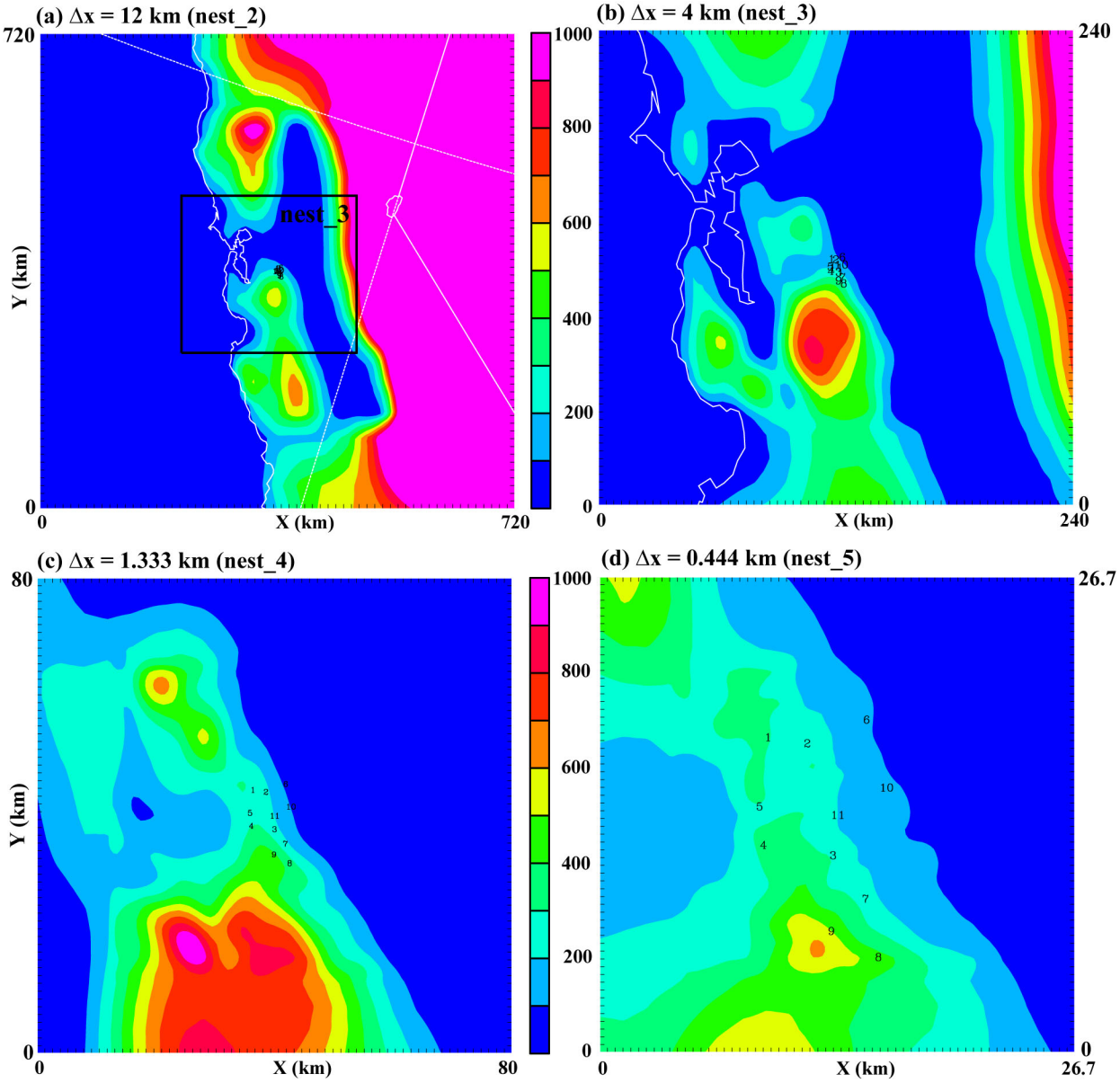

Fig. 1. Model resolved terrain height of the nested domain in unit of meter. (a) Δx = 12 km (nest_2), (b) Δx = 4 km (nest_3), (c) Δx = 1.333 km (nest_4), and (4) Δx = 0.444 km (nest_5). The letters mark the locations of tower stations used in this study (see Table 1).

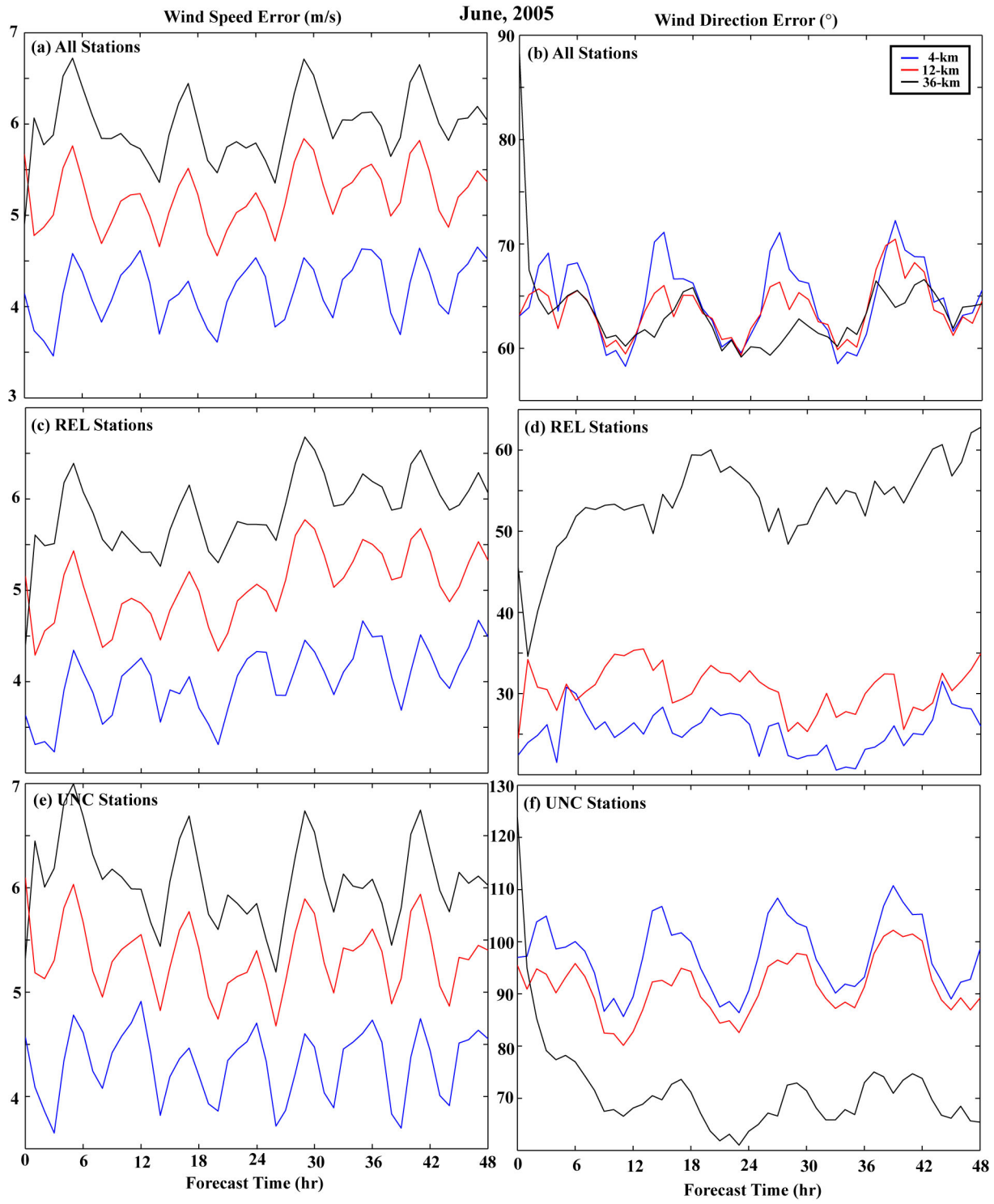

Fig. 2. Weekly mean absolute forecast errors averaged over the selected stations for June 1-7, 2005. The colored lines represent the results for different horizontal resolutions (36, 12, and 4km, respectively). The left panels are for wind speed, and the right panels for wind direction. The top panels (a and b) are the forecast errors using the measurements from all stations, the middle ones (c and d) using 5 reliable stations, and the bottom plots (e and f) using uncertain measurements from the remaining 6 stations.

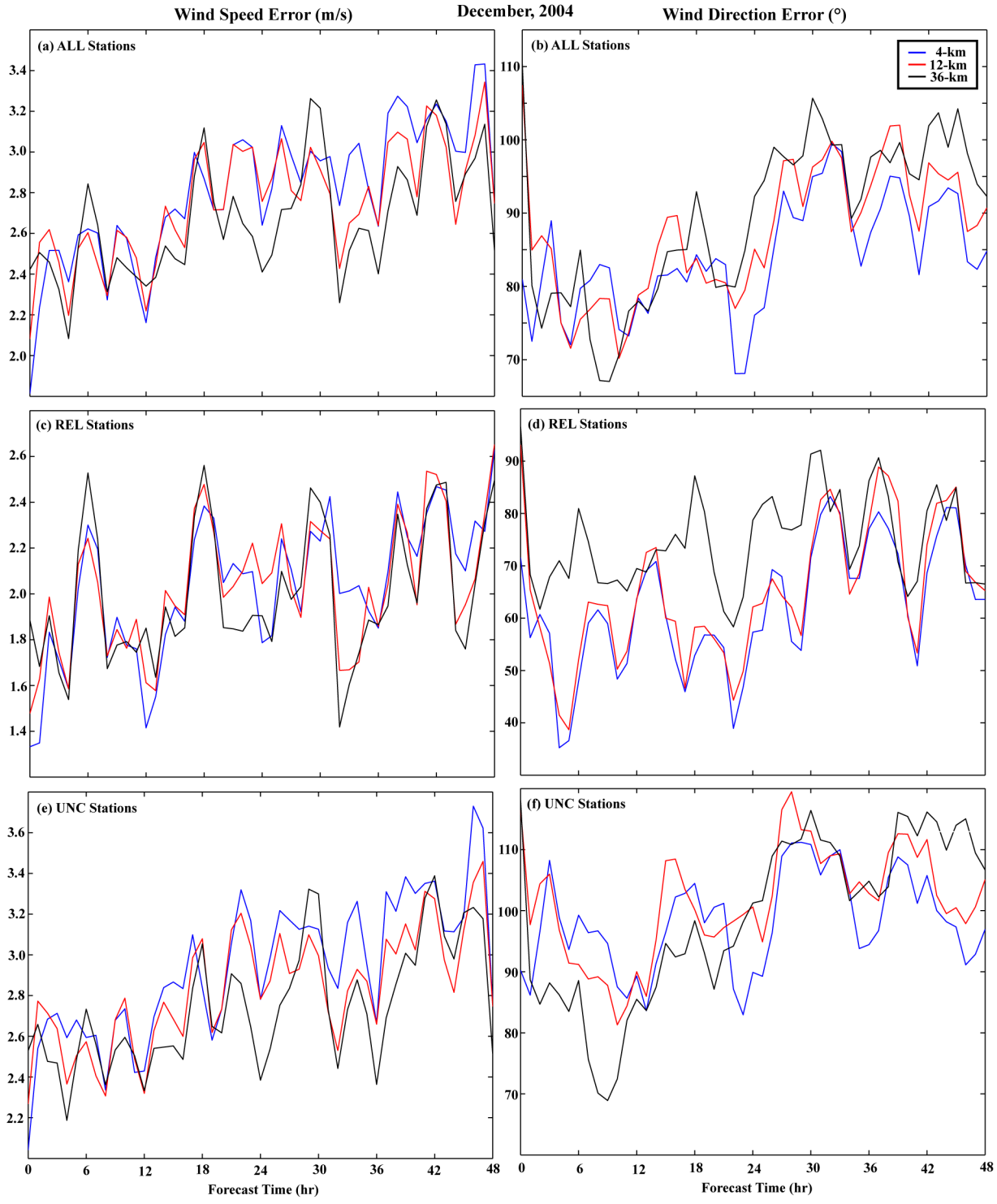

Fig. 3. As in Fig.2, except for December 2004.

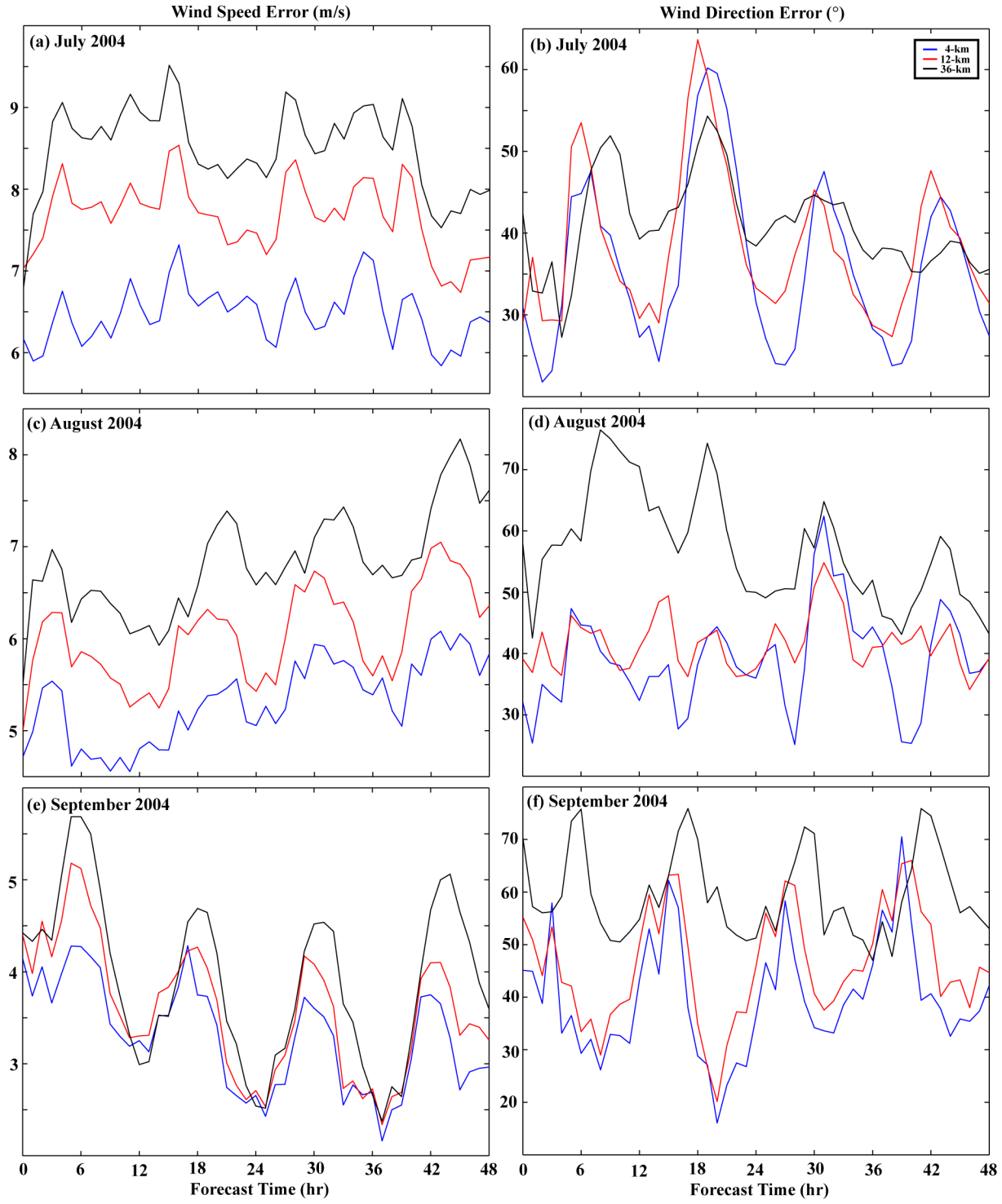

Fig. 4. As in Fig.2, except for July 2004 (a and b), August 2004 (c and d), and September 2004 (e and f), respectively.

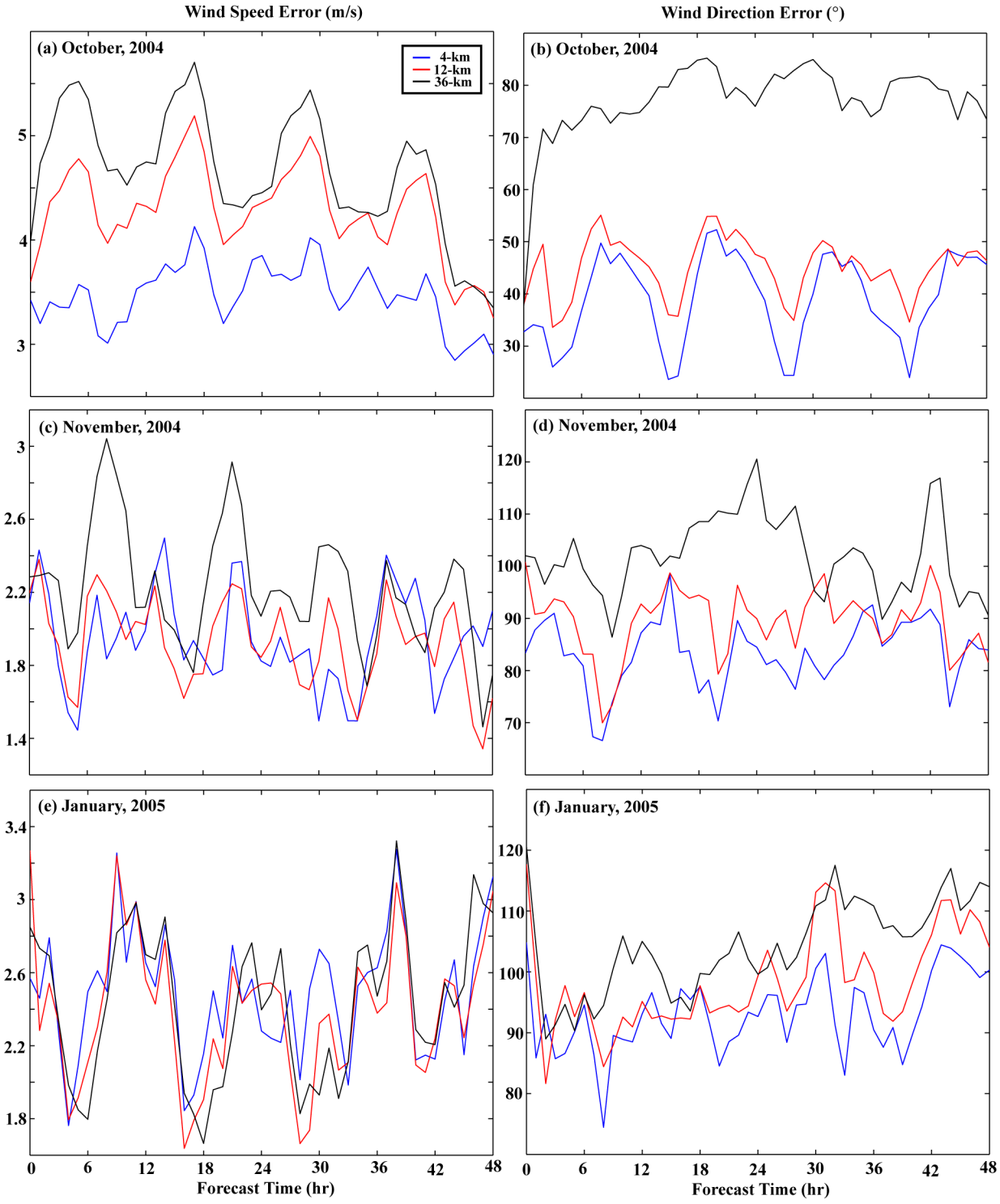

Fig. 5. As in Fig. 2, except for October 2004 (a and b), November 2004 (c and d), and January 2005 (e and f), respectively.

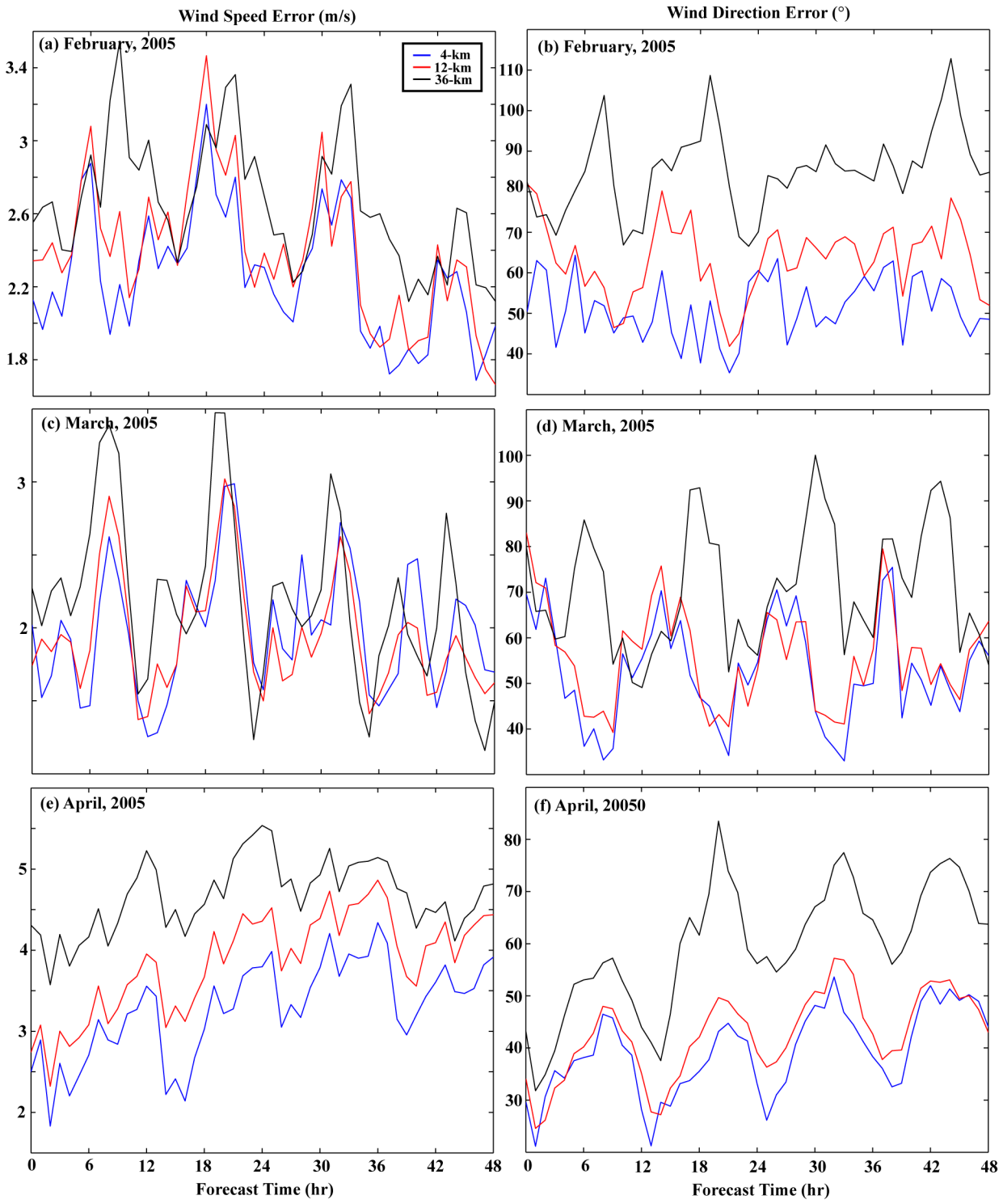

Fig. 6. As in Fig. 2, except for February 2005 (a and b), March 2005 (c and d), and April 2005 (e and f), respectively.

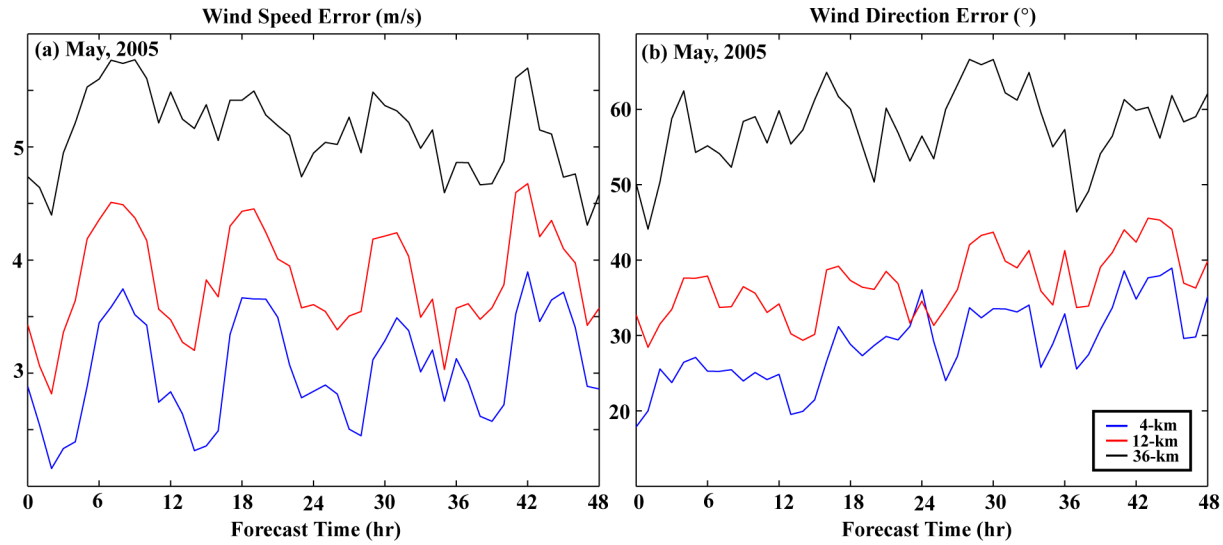

Fig. 7. As in Fig. 2, except for May 2005.

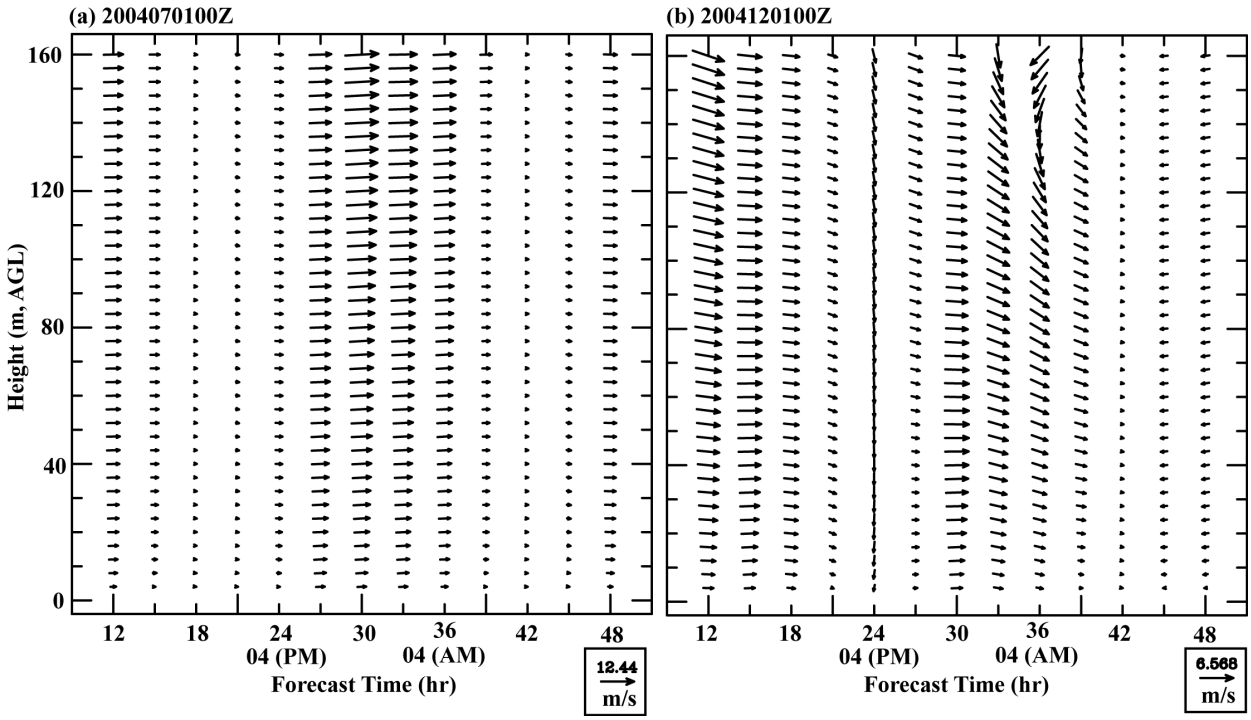

Fig. 8. Vertical profiles of forecast horizontal winds at station 127 from the nest_3 domain (Δx = 4 km), (a) from 00Z of July 01 2004, and (b) from 00Z of December 01 2004.

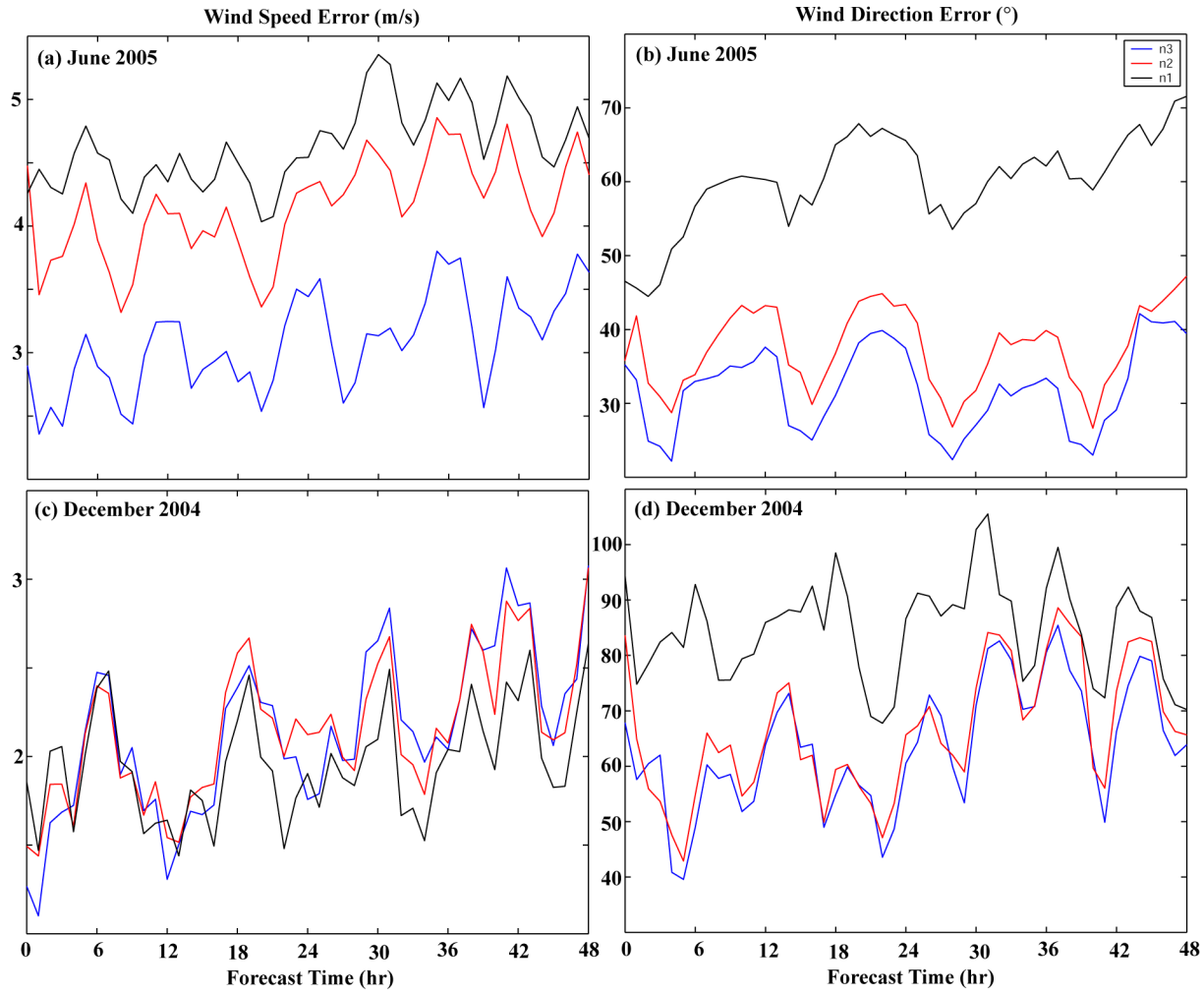

Fig. 9. (a) and (b) as in Figs. 2c and 2d, and (c) and (d) as in Figs. 3c and 3d, except for the forecast errors with the calibration of modeled terrain height.